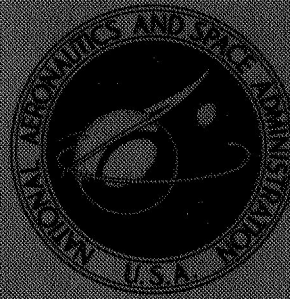
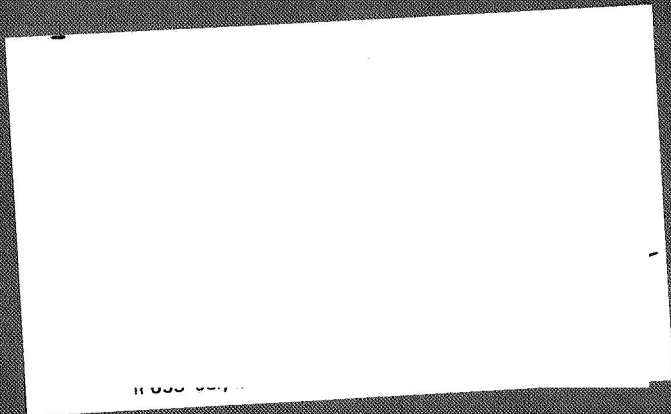


NASA TECHNICAL
MEMORANDUM



NASA TM X-1639

NASA TM X-1639



N68-30599

(ACCESSION NUMBER) 35 (PAGES)

(THRU)

(CODE) 28 (CATEGORY)

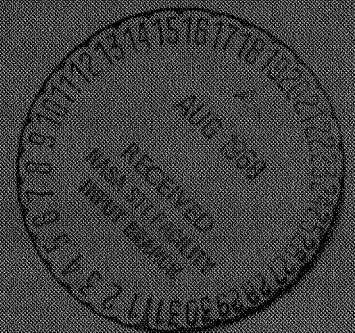
(NASA CR OR TXR OR AD NUMBER)

FACILITY FORM 602

PERFORMANCE OF A WIND TUNNEL MODEL
OF AN AERODYNAMICALLY POSITIONED
VARIABLE FLAP EJECTOR AT
MACH NUMBERS FROM 0 TO 2.0

by Fred W. Steffen and John R. Jones

Lewis Research Center
Cleveland, Ohio



PERFORMANCE OF A WIND TUNNEL MODEL OF AN AERODYNAMICALLY
POSITIONED VARIABLE FLAP EJECTOR AT MACH
NUMBERS FROM 0 TO 2.0

By Fred W. Steffen and John R. Jones

Lewis Research Center
Cleveland, Ohio

NATIONAL AERONAUTICS AND SPACE ADMINISTRATION

For sale by the Clearinghouse for Federal Scientific and Technical Information
Springfield, Virginia 22151 - CFSTI price \$3.00

ABSTRACT

A wind tunnel model of a variable flap ejector nozzle with an aerodynamically positioned shroud was evaluated over a range of Mach numbers from 0 to 2.0 at appropriate nozzle pressure ratios and statically at pressure ratios up to 26.0. Various power settings were simulated. Nozzle efficiency, pumping characteristics, boattail floating position, and boattail pressure drag were determined. The nozzle had typically high efficiencies at supersonic cruise and reheat acceleration conditions but rather low efficiency at subsonic cruise and dry acceleration conditions. The aerodynamically positioned shroud was stable at all simulated power settings and free-stream Mach numbers.

PERFORMANCE OF A WIND TUNNEL MODEL OF AN AERODYNAMICALLY
POSITIONED VARIABLE FLAP EJECTOR AT MACH
NUMBERS FROM 0 TO 2.0

by Fred W. Steffen and John R. Jones
Lewis Research Center

SUMMARY

A wind tunnel model of a variable flap ejector nozzle with an aerodynamically positioned shroud was evaluated over a range of Mach numbers from 0 to 2.0 at appropriate nozzle pressure ratios and statically at pressure ratios up to 26.0. Room temperature air was used as the primary and secondary fluid. Primary nozzle area and shroud linkage were changed during the tests to simulate geometries which would exist at subsonic cruise, dry acceleration, reheat acceleration, supersonic cruise, and idle descent power settings. Nozzle efficiency, pumping characteristics, boattail floating position, and boattail pressure drag were measured.

The nozzle had typically high efficiencies at supersonic cruise and reheat acceleration conditions but rather low performance at subsonic cruise and dry acceleration conditions. The aerodynamically positioned shroud was stable at all simulated power settings and free-stream Mach numbers.

INTRODUCTION

As part of a broad program in advanced turbojet propulsion, the Lewis Research Center is evaluating various nozzles appropriate for supersonic cruise applications. One such nozzle being considered is the variable flap ejector. For operation over a wide range of flight conditions and power settings, the variable flap ejector must be designed for extensive geometric variations of the primary nozzle and ejector shroud.

In the past, variable flap ejectors have been fitted with mechanical actuators to accomplish the geometric variations. Recently, variable flap ejectors have been designed with aerodynamically positioned shrouds and boattails. The behavior of a full-scale noz-

zle of this type under quiescent altitude conditions is reported in reference 1.

The purpose of this report is to present the results of tests made with a wind tunnel model of an aerodynamically positioned variable flap ejector over a range of free-stream Mach numbers from 0 to 2.0. Primary nozzles and shroud linkage were used which simulated configurations for subsonic cruise, dry acceleration, reheat acceleration, supersonic cruise, and idle descent power settings.

The tests were conducted in the Lewis Research Center 8- by 6-Foot Supersonic Wind Tunnel at pressure ratios appropriate to the simulated power settings and free-stream Mach numbers and in the Lewis nozzle static test facility over a range of nozzle pressure ratios up to and including supersonic cruise pressure ratio. Room temperature air was used as the primary and secondary fluid. Nozzle efficiency, pumping characteristics, boattail floating position, and boattail pressure drag were determined.

APPARATUS

Nozzles

The wind tunnel model of the variable flap ejector nozzle is shown in figure 1. In figure 1(a), the shroud is shown in the open position and in 1(b), in the partially closed position. The shroud and boattail were comprised of slotted inner flaps, inner seals, outer flaps, and outer seals. Secondary air passed around the leading edge of the inner flaps as well as through the slots in the inner flaps. Pins at the trailing edge of the shroud were used as exit area inner stops and a cable at the trailing edge of the shroud was used as the exit area outer stop. The star-shaped primary nozzle can be seen in figure 1(c).

Figure 2 is a sketch of the shroud-boattail linkage and primary nozzle. Also shown are the boattail static pressure taps. The solid lines show configuration A (used for subsonic cruise, dry acceleration, and supersonic cruise), and the dashed lines show configuration B (used for reheat acceleration and idle descent). The two configurations were achieved by making manual changes in shroud and primary nozzle geometry. For configuration A, a small primary nozzle was installed and the links at the leading edge of each flap were pinned at point a. For configuration B a large primary nozzle was installed and the links at the leading edge of each flap were pinned at point a'. The shroud and boattail moved as a four-bar linkage composed of links a-b (or a'-b), b-c, c-d, and d-a (or d-a'). In full scale, the primary nozzle and shroud-boattail linkage could be interconnected so that the shroud-boattail linkage would change with the area of the primary nozzle. The symbols shown in this figure, as well as all other symbols, are defined in appendix A.

The variation of internal ejector geometry with boattail angle for configurations A

and B is shown in figure 3, where L/D_p , D_s/D_p , and A_E/A_p are plotted as a function of β . For each configuration, the ratios L/D_p and D_s/D_p were approximately constant with β because of the linkage design. When the configuration was changed from A to B, the primary nozzle diameter was increased and, therefore, L/D_p decreased. But since the linkage was changed during the configuration change, thereby increasing D_s , the change in D_s/D_p with configuration change was small.

The maximum exit area for both configurations was approximately equal to the cross-sectional area of the forebody. Therefore, the maximum area ratio was greater for configuration A (small A_p) than for configuration B. To avoid possible low area ratio flow instability, the minimum value of A_E/A_p was restricted to 1.35 for both configurations. This restriction resulted in a smaller minimum value of A_e and a larger boattail angle for configuration A. As can be seen in figure 3, the maximum boattail angle for configuration A was 15.5° , and for configuration B, 13.0° . The change in minimum A_E was accomplished by changing the length of the inner stop pins previously shown in figure 1.

Test Facilities and Instrumentation

A photograph of the nozzle support model used for tests in the 8- by 6-Foot Supersonic Wind Tunnel is shown in figure 4. The cylindrical portion of the model was 8.5 inches (21.6 cm) in diameter. The model mounting strut, which contained the air supply tubes and the instrumentation lines, was $1\frac{3}{4}$ inches (4.43 cm) thick, with 5° half angle leading and trailing edges.

Figure 5 is a schematic view of the model showing the nozzle, nozzle adapter, and horizontal air supply bottles suspended from the vertical air supply tubes within the strut. A load cell was used to measure the net force on the free parts of the system. The equation used to calculate measured gross thrust minus drag is given in appendix B. This equation requires measured values of p_0 , p_1 , p_2 , and p_3 as well as a calculated value of the friction drag on the external surface of the model between the skin break (11.02 model diameters from the nose) and a station where the nozzle assembly was considered to begin (15.02 model diameters from the nose). The friction drag was computed using the semiempirical flat plate mean skin friction coefficient given in figure 7 of reference 2 as a function of free-stream Mach number and Reynolds number. The coefficient accounts for variations in boundary-layer thickness and profile with Reynolds number. Measurements of the boundary-layer characteristics at the aft end of this jet exit model in the 8- by 6-Foot Supersonic Wind Tunnel indicate that the profile and thickness were essentially the same as that computed for a flat plate of equal length. The strut wake appeared to affect only a localized region near the top of the model and resulted in a slightly lower local free-stream velocity than measured on the side and bottom of the model. Therefore, the results of reference 2 were used without correction for

three-dimensional flow effects or strut interference effects. A choke plate and screens were required to give a good subsonic profile to the flow approaching the nozzle. Locations of the instrumentation used to measure P_7 , P_s , and T_s are also shown in figure 5. These quantities are used in the equation for ideal thrust which is presented in appendix B. Boattail floating position was photographically recorded.

A photograph of the nozzle support and air supply system used for static tests is shown in figure 6. A schematic view of this system is shown in figure 7. A load cell was used to measure the net force on the free parts of the system. The locations of p_4 , p_5 , and p_0 , used for the calculation of measured gross thrust, as well as P_7 , P_s , and T_s , used for the calculation of ideal thrust, are shown in this figure. The equations for the calculation of measured gross and ideal thrust in the static test facility are given in appendix B also. Boattail floating position was again photographically recorded.

In order to obtain a performance reference for the wind tunnel nozzle support model, an ASME sonic nozzle, designed by the method given in reference 3, was installed and tested at $M_0 = 0$. The efficiency of this nozzle is plotted in figure 8. The data were obtained by using a value of C_D equal to 0.9930 as given in reference 3. The experimental data has a peak value of about 0.990. Peak efficiencies of 0.995 have been obtained with larger scale models of similar ASME nozzles in the static test facility. A curve of theoretical efficiency adjusted for a peak value of 0.995 is also shown in figure 8. At pressure ratios above 4, the theoretical curve and experimental data agree quite well. This result indicates that the maximum difference between the efficiency levels obtained with this model and previously established levels occurs at low pressure ratios and is no greater than -1/2 percent.

Normalized total pressure profiles of the flow approaching the primary nozzle are shown in figure 9 for the wind tunnel facility and in figure 10 for the static test facility. Except at the center the profiles are all relatively flat and similar indicating that the efficiencies and flow coefficients of both configurations in both facilities should be comparable. The low pressure readings obtained in the center of the duct at high pressure levels are not understood but may be a result of the wake from the base of the secondary air bottle. The probe gave no evidence of leakage. Because of the method used to obtain P_7 , however, an error in the center probe reading of 15 percent would cause a maximum error in P_7 of only 0.65 percent.

Boattail pressure drag was obtained from an integration of boattail static pressure over the boattail projected area. Some typical boattail pressure coefficient distributions are shown in figure 11. Because of the small number of pressure measurements in each axial row, the minimum pressure which would occur close to the boattail shoulder may not have been properly accounted for in the integration. A comparison with well-defined boattail pressure distributions from reference 4 is shown in figure 11(c). Also, the circumferential variations of pressure coefficients shown in figure 11 (which are typical of the variations at all Mach numbers) did not indicate any appreciable mounting strut effect.

PROCEDURE

Test Procedure in the 8- by 6-Foot Supersonic Wind Tunnel

The schedule shown in figure 12 was used as a guide for setting pressure ratio over the range of Mach numbers from 0 to 2.0 for each power setting. At each Mach number, data were taken at several pressure ratios around the values shown in figure 12. At each pressure ratio, corrected secondary weight flow ratio was varied from 0 to 0.10 for the dry acceleration, reheat acceleration, and subsonic cruise power settings; for the idle descent power setting, the corrected secondary weight flow ratio was set at approximately 0.14.

Test Procedure in the Static Test Facility

Configurations A and B were both tested over a range of pressure ratios from 1.5 to 26 for corrected secondary weight flow ratios from 0 to 0.14. The performance of configuration A at a pressure ratio of 26 with a corrected secondary weight flow ratio of 0.02 was used as a basis for supersonic cruise performance.

Data Presentation Procedure

The basic data, consisting of nozzle efficiencies and pumping characteristics, are presented in appendix C. These data were used in conjunction with the pressure ratio schedule of figure 12 to present the nozzle performance in the RESULTS AND DISCUSSION section. Supersonic cruise efficiency is obtained from the static efficiency reduced by 0.003 to account for an estimated friction drag on the boattail. The friction drag coefficient used for this estimate was obtained from reference 2 for a Reynolds number of 6×10^7 and a Mach number of 2.7.

RESULTS AND DISCUSSION

The nozzle efficiency of the variable flap ejector over a range of free-stream Mach numbers at several simulated power settings is shown in figure 13. The corrected secondary weight flow ratios chosen for the supersonic cruise, subsonic cruise, and reheat acceleration power settings were considered typical of the values which would be used for supersonic cruise vehicles. The corrected secondary weight flow ratio of 0.01 used for

the dry acceleration performance was about the maximum amount that the ejector could pump assuming free-stream inlets were utilized with reasonable total pressure losses. Peak nozzle efficiency occurred at supersonic cruise and had a value of 0.975. The lowest efficiency occurred with a subsonic cruise power setting at $M_0 = 0.92$ and had a value of about 0.855.

Because of the small number of data points taken at the idle descent power setting and because of the random variations in secondary flow at this power setting, the idle descent performance is not included in figure 13 but is listed separately in table I.

Figure 14 presents a comparison of nozzle efficiency at various power settings with and without external flow. The differences in nozzle efficiency are caused by boattail pressure drag, friction drag, and the interaction of the external and internal flows. The largest differences occur at subsonic cruise where the thrust level is low and the boattail angles are high.

It should be noted that for all the conditions shown in figure 14, except subsonic cruise at $M_0 = 0.81$, the boattail floating position was unaffected by external flow. For subsonic cruise at $M_0 = 0.81$, the boattail angle observed statically was about 1° more than with external flow.

The portion of the external flow effect due to boattail pressure drag is shown in figure 15, which is a plot of the boattail pressure drag loss against Mach number for three simulated power settings. Boattail pressure drag loss is defined as the ratio of the measured boattail pressure drag to the sum of the ideal primary and secondary thrust. At subsonic cruise pressure ratios, the boattail pressure drag loss attains a maximum value of 0.06 because of the low value of ideal thrust and the high drag resulting from a high boattail angle.

The observed boattail angles for four simulated power settings, including idle descent, are shown as a function of Mach number in figure 16. The highest boattail angles occur at dry acceleration power settings up to a Mach number of 0.5 and at subsonic cruise power settings for Mach numbers from 0.81 to 0.91. A minimum boattail angle of about 1° is reached at $M_0 = 1.97$ with a reheat acceleration power setting. A boattail angle of 0° was observed at simulated supersonic cruise operation, that is, $P_7/p_0 = 26$ and $M_0 = 0$.

Boattail angle is plotted as a function of nozzle pressure ratio for a range of free-stream Mach numbers in figure 17. Data for both configurations A and B are shown. The boattail angle is shown to be primarily a function of nozzle pressure ratio, except at low values of nozzle pressure ratio, where the boattail angle also becomes dependent on free-stream Mach number. No change in boattail angle with corrected secondary weight flow ratio was detectable within the scatter of the data.

The ratio of the secondary total pressure to free-stream total pressure required for corrected secondary weight flow ratios at various free-stream Mach numbers and power

settings is shown in figure 18. At subsonic cruise power settings (fig. 18(a)), the secondary total pressure required for a corrected secondary flow ratio of 0.04 is only 0.63 of the free-stream total pressure. At subsonic speeds with higher power settings, however, the total pressure of the secondary flow entering the ejector becomes more critical. At the dry acceleration power setting at Mach 0.91 (fig. 18(b)), a secondary total pressure of 0.92 of free-stream total pressure is required for a corrected secondary weight flow ratio of 0.01. At the reheat acceleration power setting at Mach 0.91 (fig. 18(c)), a secondary total pressure of 0.94 of free-stream total pressure is required for a corrected secondary weight flow ratio of 0.04. These data indicate that auxiliary inlets close to the ejector may be required to provide sufficient secondary total pressure.

The division of the secondary flow around the leading edge of the shroud, through the slots in the flaps, and between the flaps and seals was not determined. Unpublished data with larger scale models of this ejector indicate that about 10 percent of the secondary flow passes through the slots. Although the design and fabrication of the model shroud were carefully controlled to minimize leakage of the secondary flow through the seals, the magnitude of the actual seal leakage was not determined nor was it determined if the leakage was representative of full-scale leakage with elevated wall temperatures.

The floating shroud was stable at all simulated power settings and free-stream conditions. It should be remembered, however, that the frictional forces in a nozzle of this type may influence its dynamic stability characteristics. No attempt was made in the design or fabrication of this model to simulate or scale the frictional forces which would occur in a full-scale nozzle operating at elevated temperatures for extended periods of time.

During some brief inadvertent operation with the small primary nozzle at a pressure ratio of 1.1, a Mach number of 0.8, and a corrected secondary weight flow ratio of 0, a gentle low frequency instability was noticed. Although the combination of geometry and operating conditions was unrealistic, the occurrence suggested that the stability of an aerodynamically positioned nozzle may be most critical during low power operation and that it is important to test an aerodynamically positioned nozzle for stability characteristics at the lowest power settings anticipated.

SUMMARY OF RESULTS

A wind tunnel model of a variable flap ejector nozzle with an aerodynamically positioned shroud was evaluated at Mach numbers from 0 to 2.0 at simulated power settings for supersonic cruise, subsonic cruise, reheat acceleration, dry acceleration, and idle descent.

Nozzle efficiency (excluding idle descent efficiency) varied from a high of 0.975 at

supersonic cruise to a low of 0.855 at subsonic cruise. At subsonic cruise, the boattail drag amounted to about 6 percent of ideal thrust. Pumping characteristics at subsonic flight conditions with high power settings were marginal and suggested that an auxiliary inlet for secondary air may be required.

The aerodynamically positioned shroud was stable at all Mach numbers and simulated power settings. At all simulated power settings except idle and cruise at $M_0 = 0.8$, the shroud position was dictated by internal pressures and was independent of free-stream and secondary flow effects.

Lewis Research Center,
National Aeronautics and Space Administration,
Cleveland, Ohio, April 29, 1968,
126-15-02-10-22.

APPENDIX A

SYMBOLS

| | |
|--|---|
| <p>A area</p> <p>C_D primary nozzle flow coefficient</p> <p>C_p boattail pressure coefficient, $(p - p_0)/q_0$</p> <p>D drag</p> <p>D_E shroud exit diameter</p> <p>D_p primary nozzle diameter</p> <p>D_s internal shroud diameter</p> <p>$D_{\beta p}$ boattail pressure drag</p> <p>F jet thrust</p> <p>F_{LC} force on load cell</p> <p>g gravitational constant</p> <p>L ejector shroud length</p> <p>M Mach number</p> <p>P total pressure</p> <p>p static pressure</p> <p>q dynamic pressure, $(\rho_0 V_0^2)/2$</p> <p>R total radius</p> <p>r local radius</p> <p>T total temperature</p> <p>V velocity</p> <p>W weight flow rate</p> <p>β boattail angle</p> | <p>ρ mass density</p> <p>τ temperature ratio, T_s/T_p</p> <p>ω weight flow ratio, W_s/W_p</p> <p>Subscripts:</p> <p>E exit</p> <p>f friction</p> <p>I ideal</p> <p>L local</p> <p>L.S. labyrinth seal</p> <p>p primary</p> <p>s secondary</p> <p>S.L. lip static</p> <p>0 free stream</p> <p>1 wind tunnel model station 1 (see fig. 5)</p> <p>2 wind tunnel model station 2 (see fig. 5)</p> <p>3 wind tunnel model station 3 (see fig. 5)</p> <p>4 static test facility station 4 (see fig. 6)</p> <p>5 static test facility station 5 (see fig. 6)</p> <p>7 inlet to primary nozzle</p> |
|--|---|

APPENDIX B

CALCULATION OF MEASURED GROSS THRUST AND IDEAL THRUST

8- by 6-Foot Supersonic Wind Tunnel

Measured gross thrust minus drag was obtained from the following equation:

$$F - D = F_{LC} + A_1(p_1 - p_0) + A_2(p_2 - p_0) + A_3(p_3 - p_0) + D_f \quad (B1)$$

The force applied to the load cell F_{LC} was obtained from the electrical output of the load cell and a calibration of the electrical output as a function of a known axial load applied to the primary nozzle mounting flange. The friction drag D_f is the computed friction drag on the outside of the model between the skin break and a station 1.6 body diameter upstream of the exit plane. The latter station was chosen as being typical of a station at which the nozzle installation (including thrust reversal doors) would begin.

The ideal primary thrust is defined as:

$$F_{Ip} = \frac{W_p}{g} V_{Ip} \quad (B2)$$

where

$$\frac{W_p}{g} V_{Ip} = \frac{\left[0.91885 \sqrt{5.0 \left[\left(\frac{P_7}{P_{SL}} \right)^{0.28571} - 1.0 \right]} \right]}{\left(1.0 + 0.2 \left\{ 5.0 \left[\left(\frac{P_7}{P_{SL}} \right)^{0.28571} - 1.0 \right] \right\} \right)^3} \left[3.40745 \sqrt{1 - \left(\frac{P_0}{P_7} \right)^{0.28571}} \right] P_7 A_p C_D \quad (B3)$$

Values of C_D were obtained from previous tests of larger scale star-shaped primary nozzles. For configuration A, $C_D = 0.9810$ and for configuration B, $C_D = 0.9900$. The secondary total pressure was used as the lip static pressure and the value of P_7/P_{SL} was limited to a maximum of 1.8929.

The ideal secondary thrust is defined as:

$$F_{Is} = \frac{W_s V_{Is}}{g} = W_s \left[3.40745 \sqrt{1 - \left(\frac{P_0}{P_s} \right)^{0.28571}} \right] \sqrt{T_s} \quad (B4)$$

The secondary weight flow W_s was measured with a sharp-edge ASME orifice, using standard ASME orifice flow coefficients as given in reference 2.

For conditions where $P_s \leq p_0$, F_{Is} was considered to be zero. Basic efficiency data calculated with this consideration is indicated by flagged symbols in appendix C.

Static Test Facility

Measured gross thrust was obtained from the following equation:

$$F = \frac{W}{g} V_4 - A_4(p_5 - p_4) + A_{L.S.}(p_5 - p_0) - F_{LC} \quad (B5)$$

The quantity $(W/g)V_4 - A_4(p_5 - p_4)$ was obtained as a function of the static to total pressure ratio at the flow-metering station from facility calibrations. The effective area of the duct under the labyrinth seals $A_{L.S.}$ was also obtained from facility calibrations. The force required to maintain equilibrium F_{LC} was obtained from the pneumatic output of the Hagan load cell and a calibration of the pneumatic output as a function of a known axial load applied to the nozzle mounting flange. As in the wind tunnel facility, ideal primary thrust and ideal secondary thrust were obtained by use of equations (B2), (B3), and (B4).

APPENDIX C

NOZZLE EFFICIENCY AND PUMPING DATA

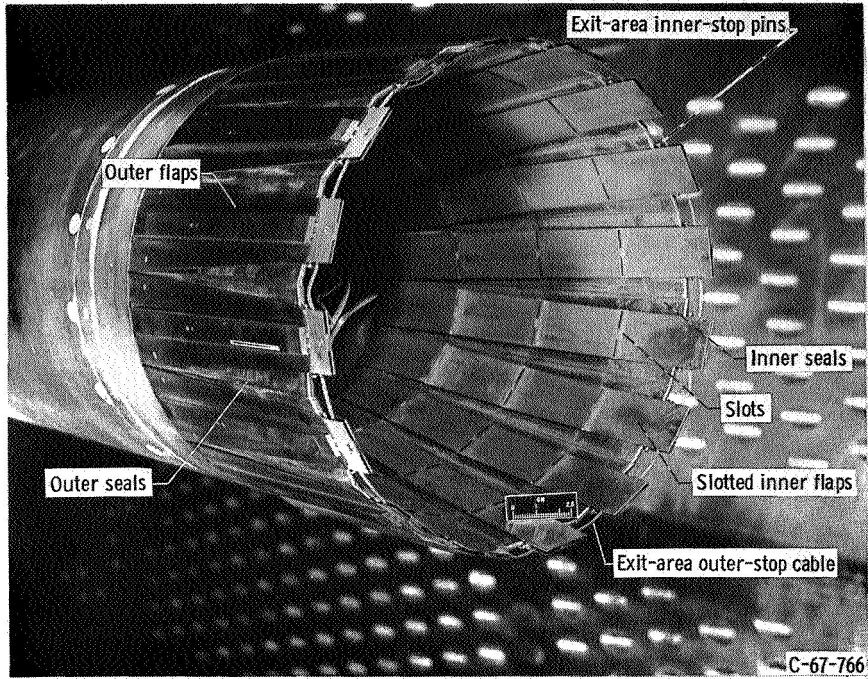
This appendix contains all of the nozzle efficiency and pumping data taken during the program. Figure 19 is a plot of the nozzle efficiency of configuration A as a function of nozzle pressure ratio with Mach number as a parameter. Figure 20 is the same type of plot for configuration B. Figure 21 is a plot of the ratio of the secondary total pressure to primary total pressure required by configuration A for various corrected secondary weight flow ratios with Mach number as a parameter. Figure 22 is the same type of plot for configuration B.

REFERENCES

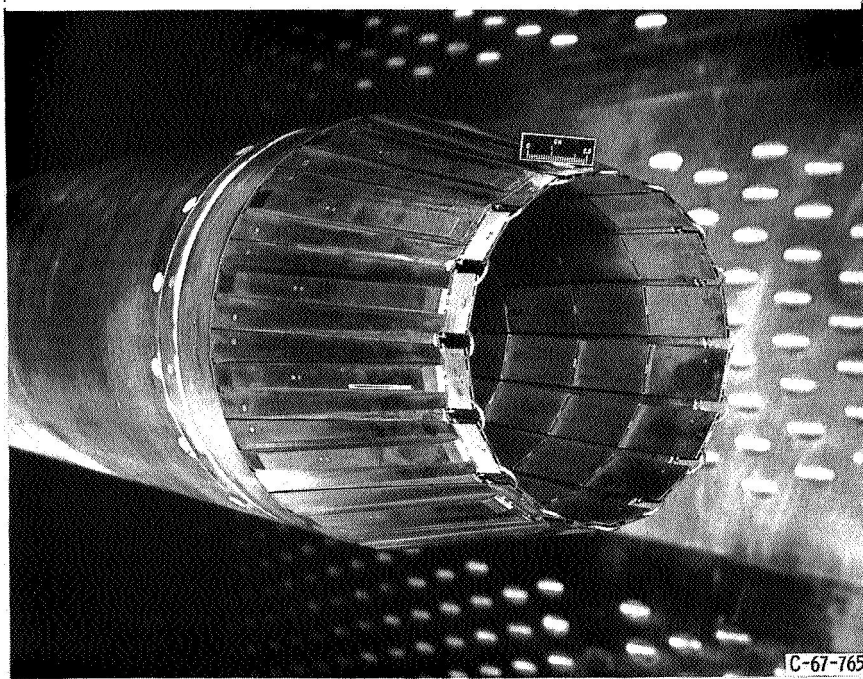
1. Edmunds, E. W.: Operational Investigation of an Aerodynamic-Positioned Secondary Exhaust Nozzle for a Turbojet Engine in an Altitude Test Cell. Aro, Inc. (AEDC-TR-66-76, DDC No. AD-481722), May 1966.
2. Smith, K. G.: Methods and Charts for Estimating Skin Friction Drag in Wind Tunnel Tests With Zero Heat Transfer. Rep. ARC-CP-824, Aeronautical Research Council, Great Britain, 1965. (Available from DDC as AD-487132.)
3. Anon.: Fluid Meters, Their Theory and Application. Fifth ed., ASME, 1959.
4. Shrewsbury, George D.: Effects of Boattail Juncture Shape on Pressure Drag Coefficients of Isolated Afterbodies. NASA TM X-1517, 1968.

TABLE I. - IDLE DESCENT PERFORMANCE

| Free-stream Mach number, M_0 | Nozzle pressure ratio, P_7/P_0 | Nozzle efficiency, $\frac{F - D}{F_{I,p} + F_{I,s}}$ | Corrected secondary weight flow ratio, $\omega\sqrt{\tau}$ | Secondary to primary total pressure ratio, P_s/P_7 | Ratio of secondary total pressure to free-stream total pressure, P_s/P_0 |
|--------------------------------|----------------------------------|--|--|--|--|
| | | | | | |
| 0.56 | 1.24 | 0.76 | 0.13 | 0.79 | 0.79 |
| .56 | 1.08 | .44 | .09 | .91 | .79 |
| .82 | 1.26 | .66 | .13 | .78 | .63 |
| .82 | 1.13 | .48 | .13 | .86 | .63 |
| .91 | 1.28 | .61 | .13 | .76 | .57 |
| .91 | 1.16 | .42 | .11 | .83 | .56 |
| 1.01 | 1.57 | .67 | .14 | .60 | .49 |
| 1.01 | 1.25 | .46 | .13 | .75 | .49 |
| 1.06 | 1.50 | .52 | .14 | .58 | .43 |
| 1.06 | 1.28 | .33 | .14 | .69 | .44 |
| 1.27 | 2.42 | .71 | .18 | .54 | .49 |
| 1.27 | 1.69 | .54 | .14 | .51 | .33 |
| 1.57 | 2.16 | .63 | .16 | .48 | .26 |
| 1.77 | 3.36 | .74 | .17 | .51 | .31 |
| 1.97 | 4.16 | .81 | .19 | .53 | .30 |

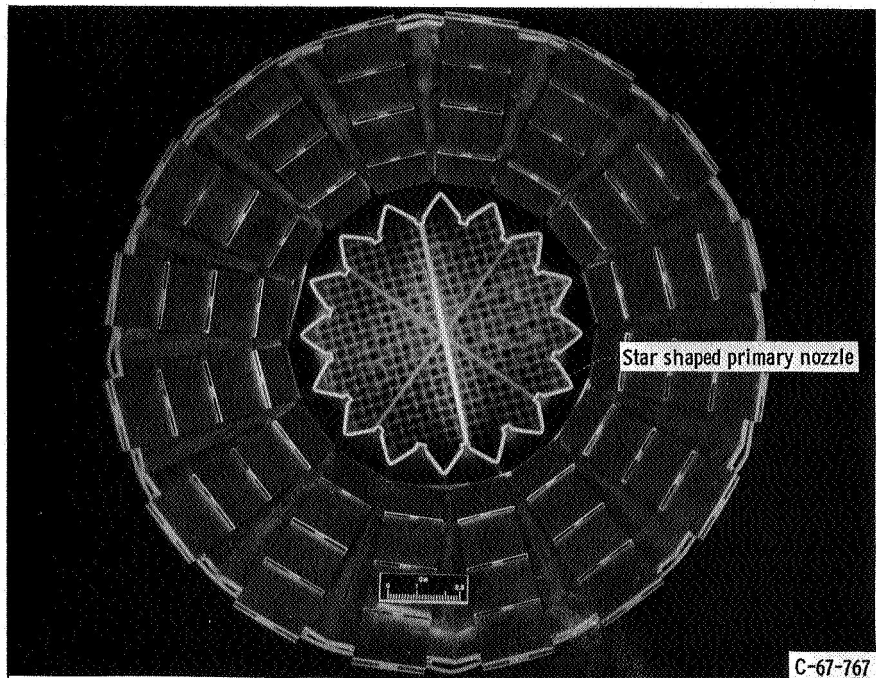


(a) Shroud open.



(b) Shroud partially closed.

Figure 1.- Variable flap ejector model.



(c) Open shroud and star shaped primary nozzle.

Figure 1. - Concluded.

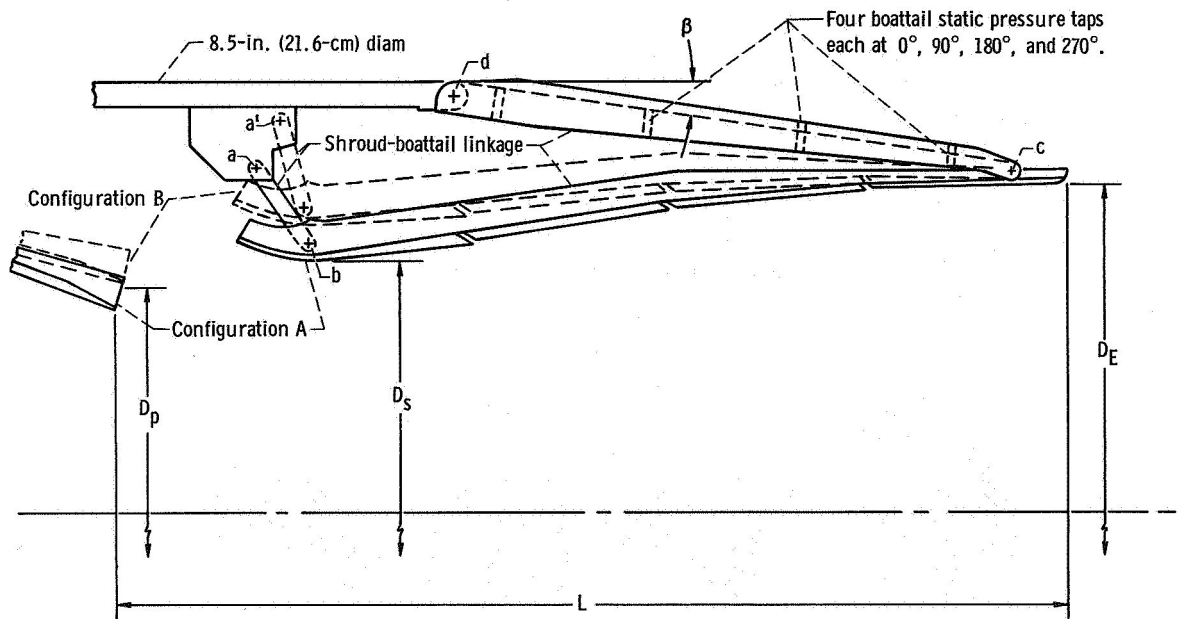


Figure 2. - Variable flap ejector geometry, linkage, and instrumentation.

CD-9816-28

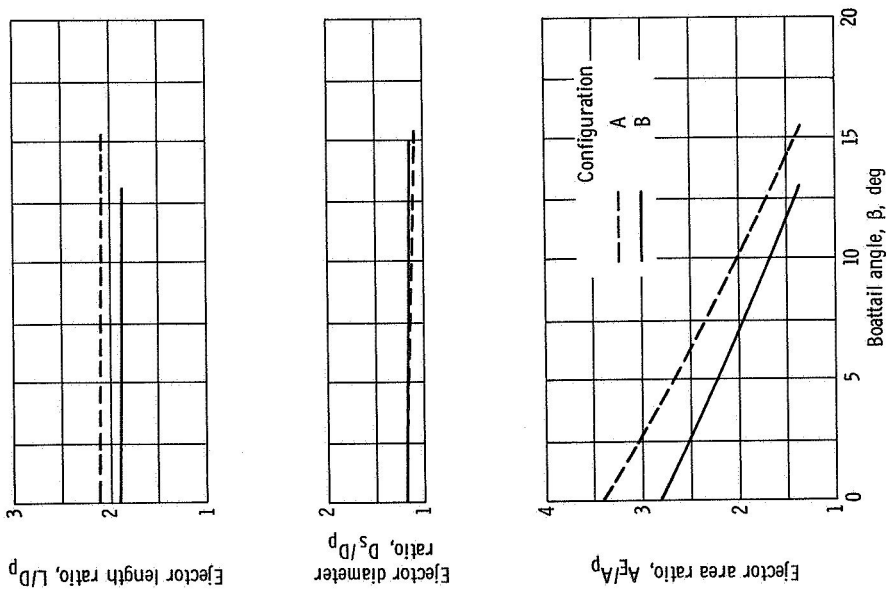


Figure 3. - Variation of internal ejector geometry with boattail angle.

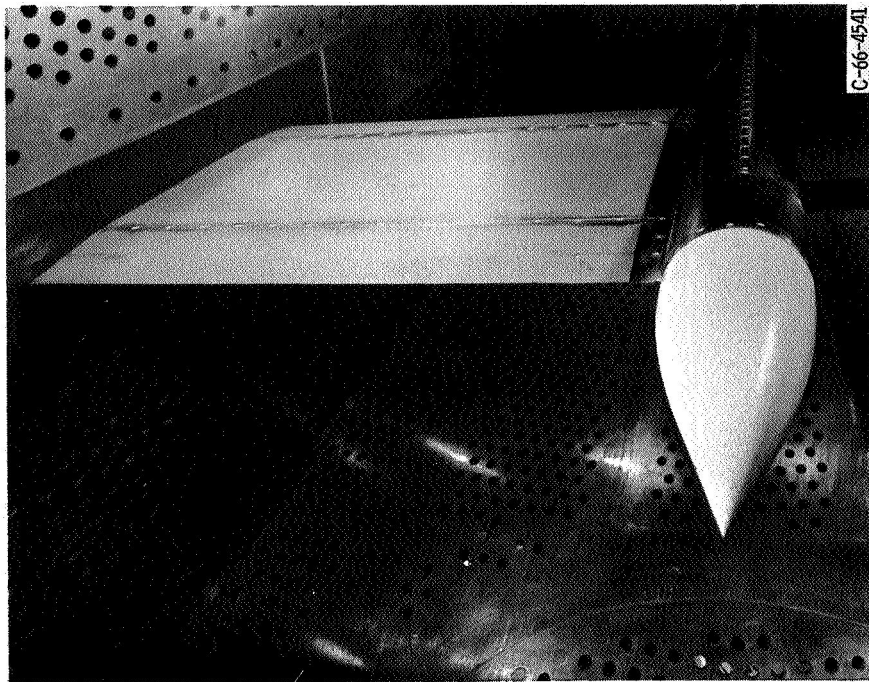


Figure 4. - Nozzle support model used for wind tunnel tests.

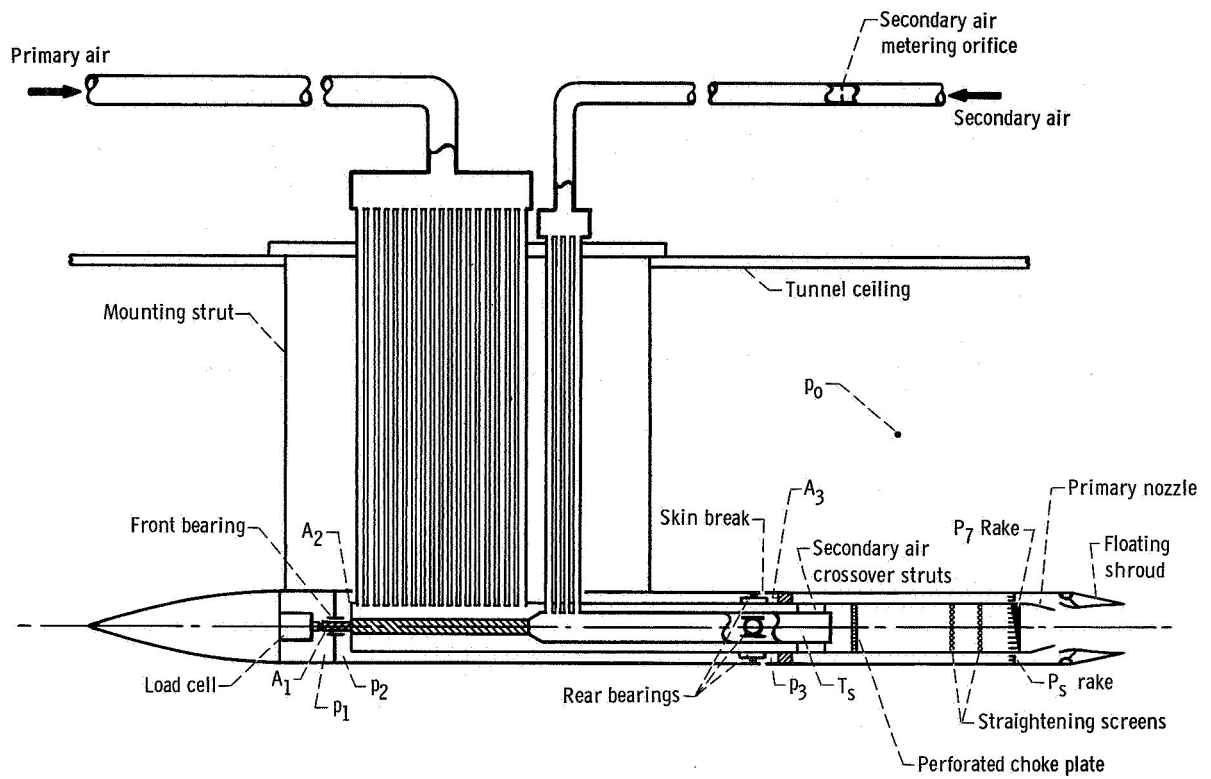


Figure 5. - Schematic view of nozzle support model and air supply system used for wind tunnel tests.

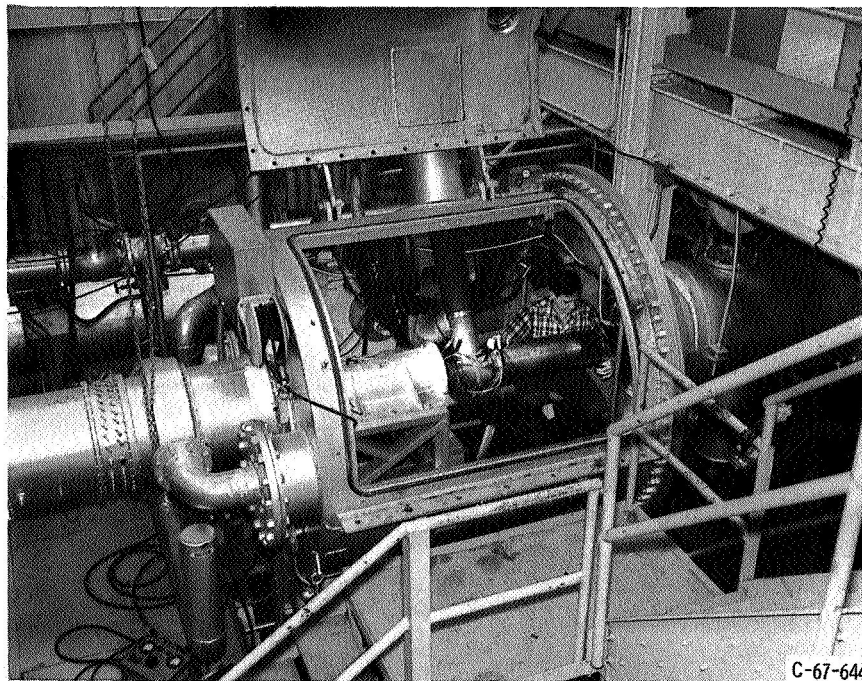
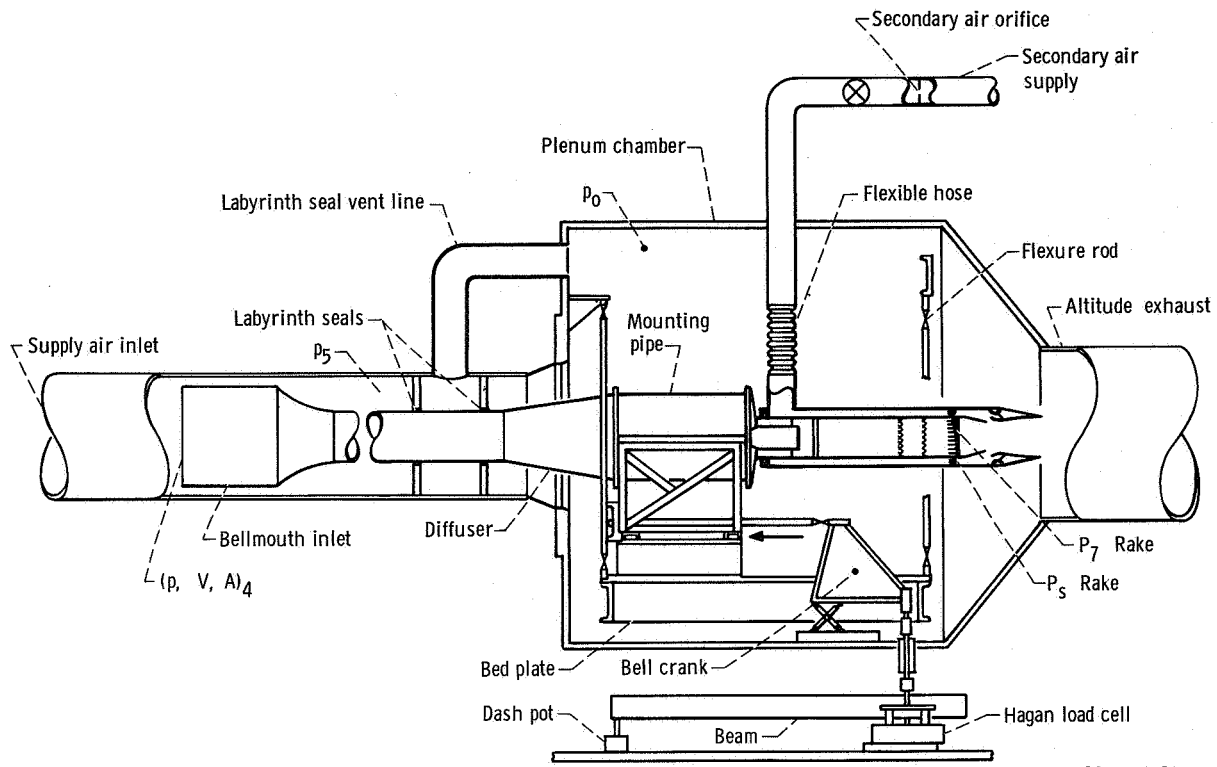


Figure 6. - Nozzle support and air supply system used during static tests.



CD-9818-28

Figure 7. - Schematic view of nozzle support and air supply system used during static tests.

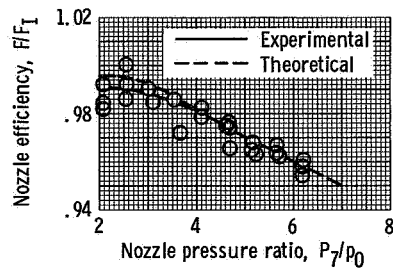


Figure 8. - Performance of A.S.M.E. sonic nozzle installed on wind tunnel support model.

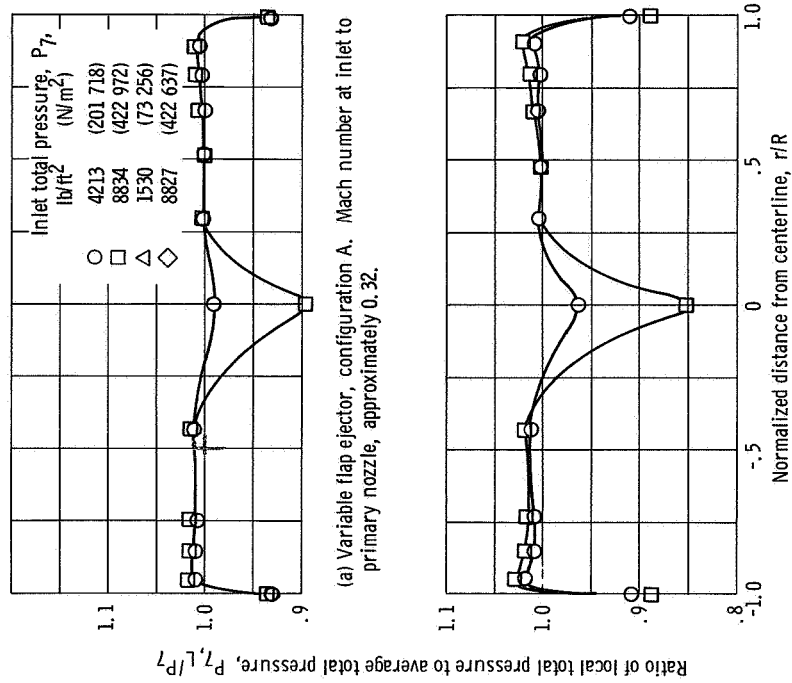


Figure 9. - Normalized total pressure profiles at station 7 in wind tunnel nozzle support model.

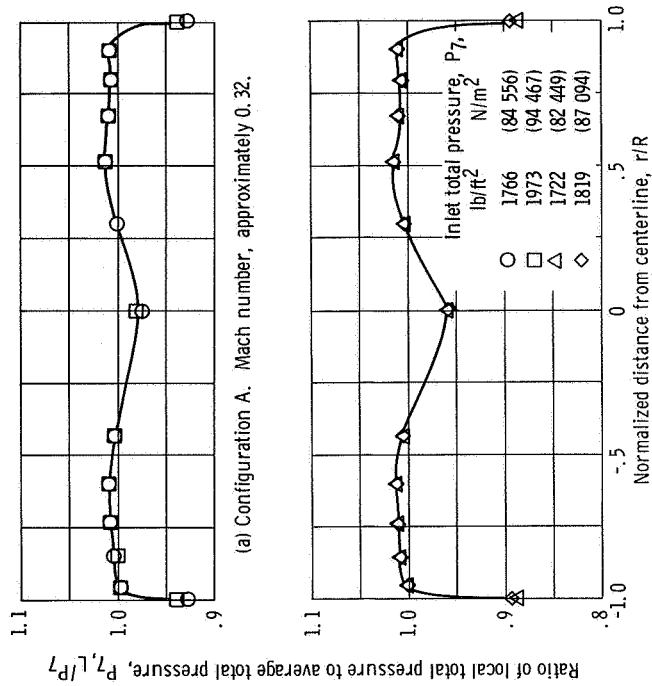
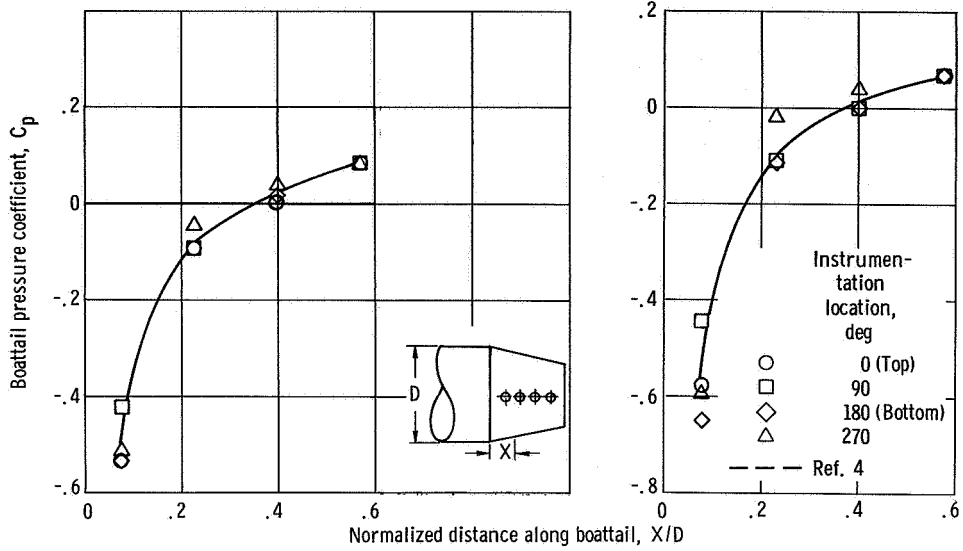
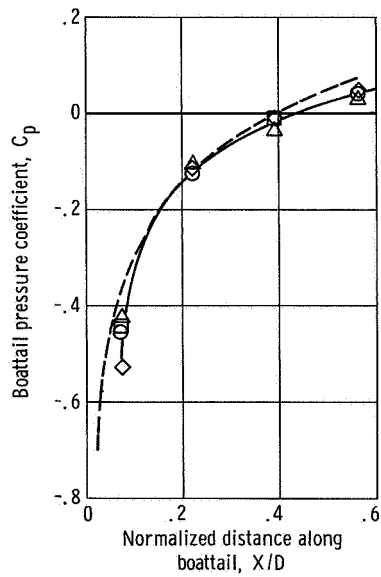


Figure 10. - Normalized total pressure profiles at station 7 in nozzle static test facility.



(a) Reheat acceleration with 12° boattail and $P_7/P_0 = 5.6$.

(b) Dry acceleration with 12° boattail and $P_7/P_0 = 5.9$.



(c) Subsonic cruise with 15° boattail and $P_7/P_0 = 3.2$.

Figure 11. - Axial variation of pressure coefficient on boattail at Mach 0.9.

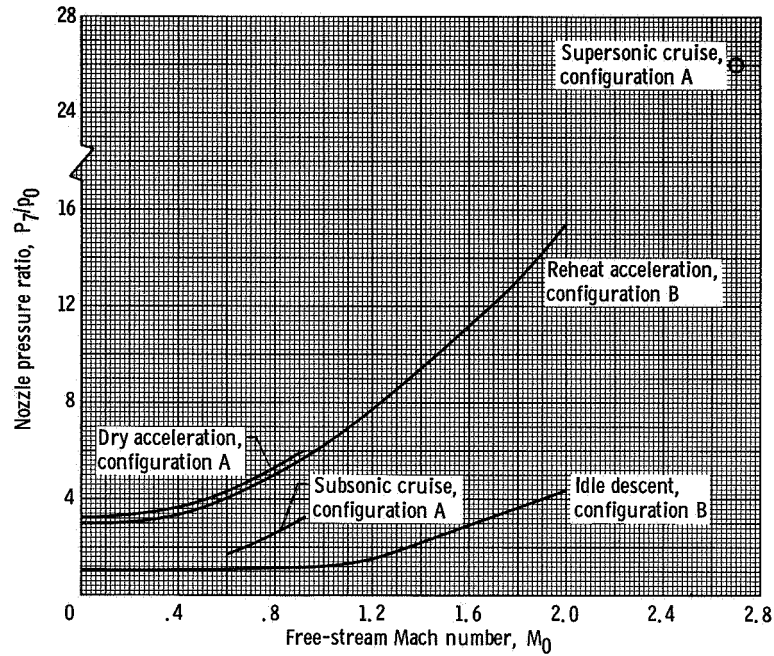


Figure 12. - Schedule of nozzle pressure ratio with free-stream Mach number for four simulated power settings.

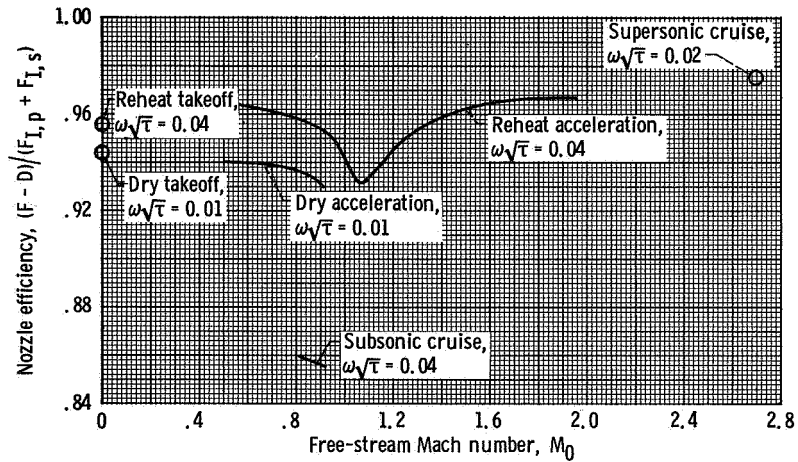
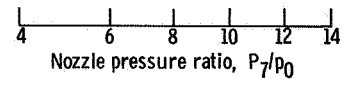
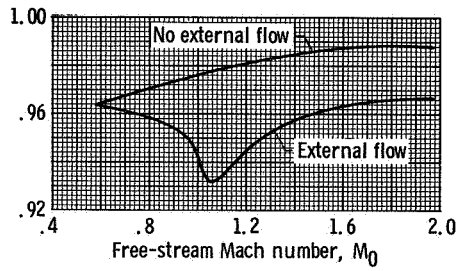
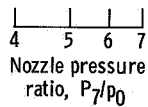
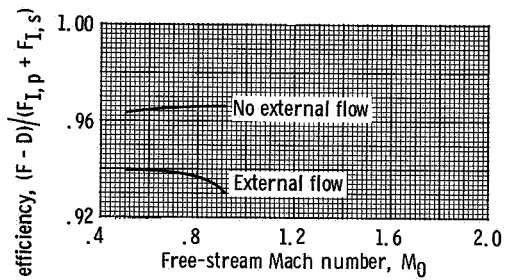


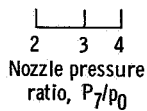
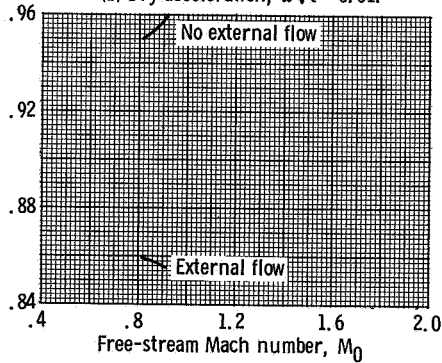
Figure 13. - Efficiency of variable flap ejector.



(a) Reheat acceleration, $\omega\sqrt{\tau} = 0.04$.



(b) Dry acceleration, $\omega\sqrt{\tau} = 0.01$.



(c) Subsonic cruise, $\omega\sqrt{\tau} = 0.04$.

Figure 14. - Comparison of nozzle efficiency with and without external flow.

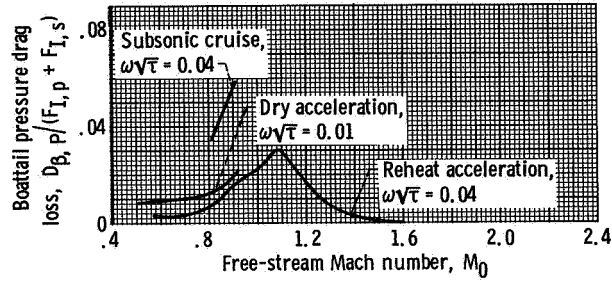


Figure 15. - Boattail pressure drag loss for variable flap ejector.

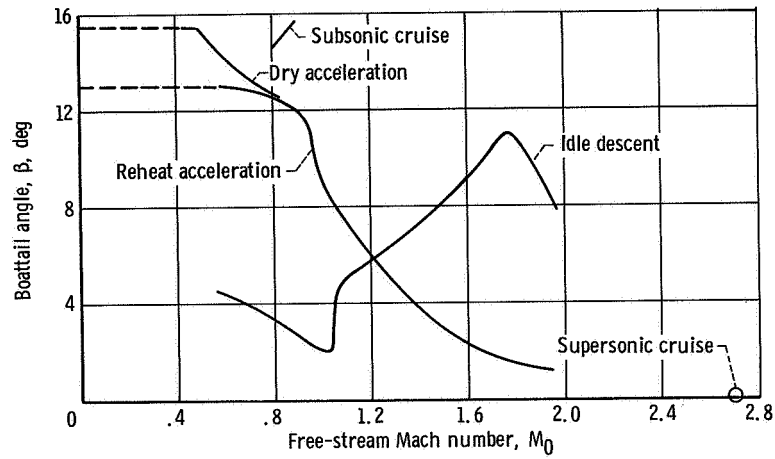


Figure 16. - Variation of boattail angle with Mach number for four simulated power settings.

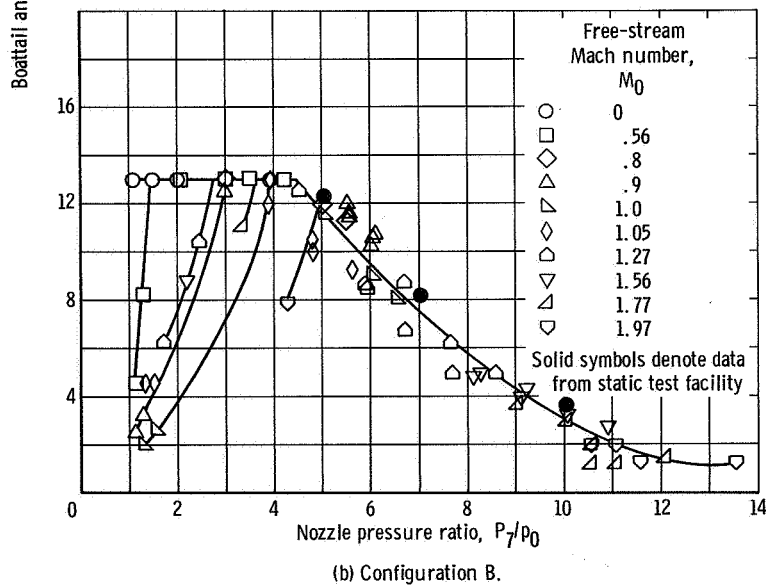
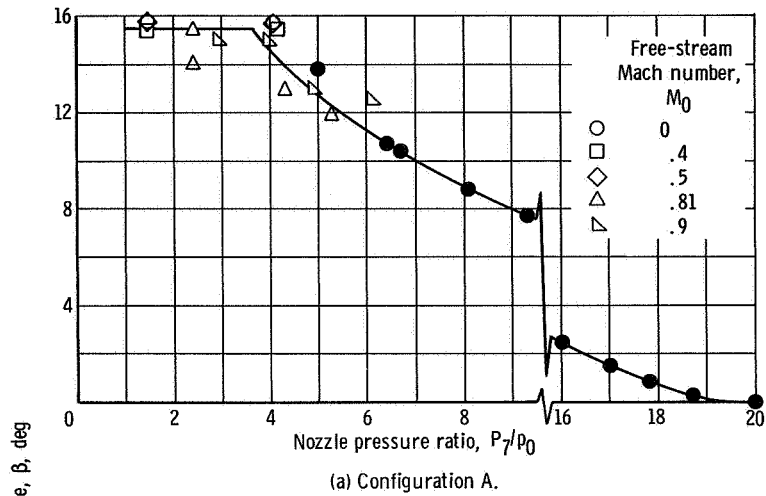
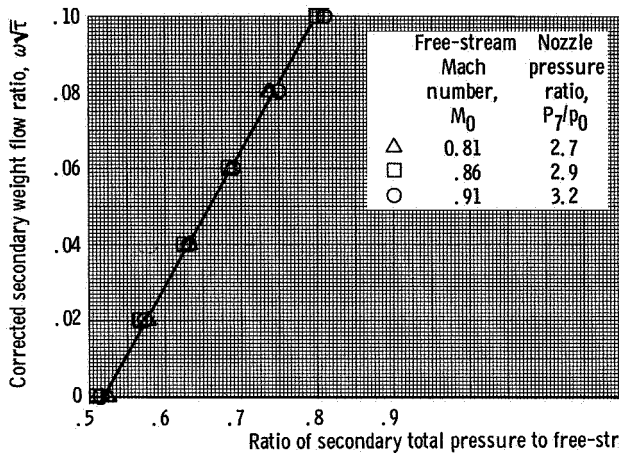
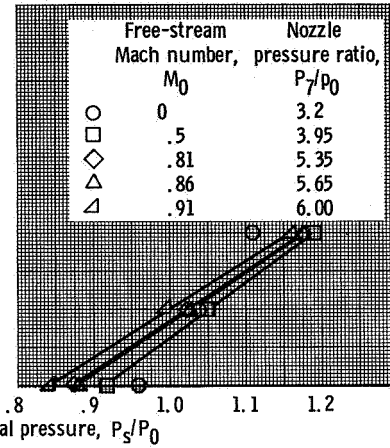


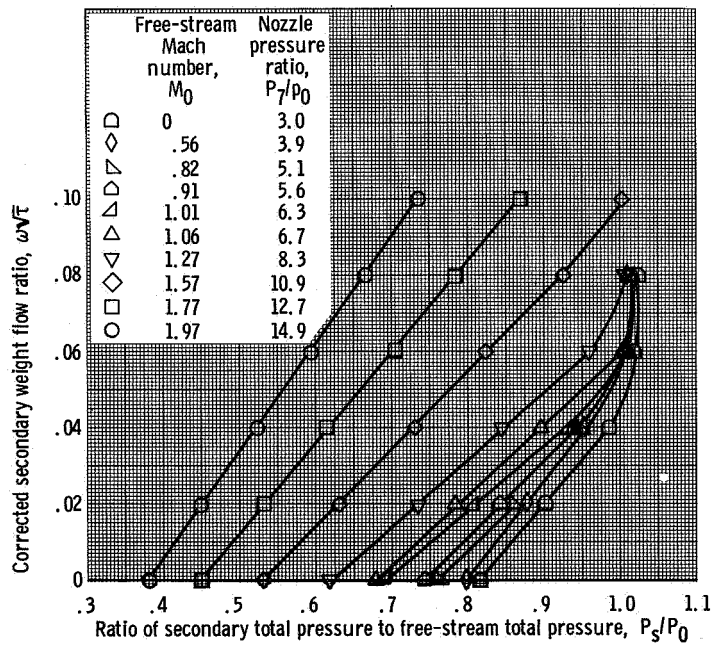
Figure 17. - Variation of boattail angle with nozzle pressure ratio over range of free-stream Mach numbers.



(a) Subsonic cruise, configuration A.

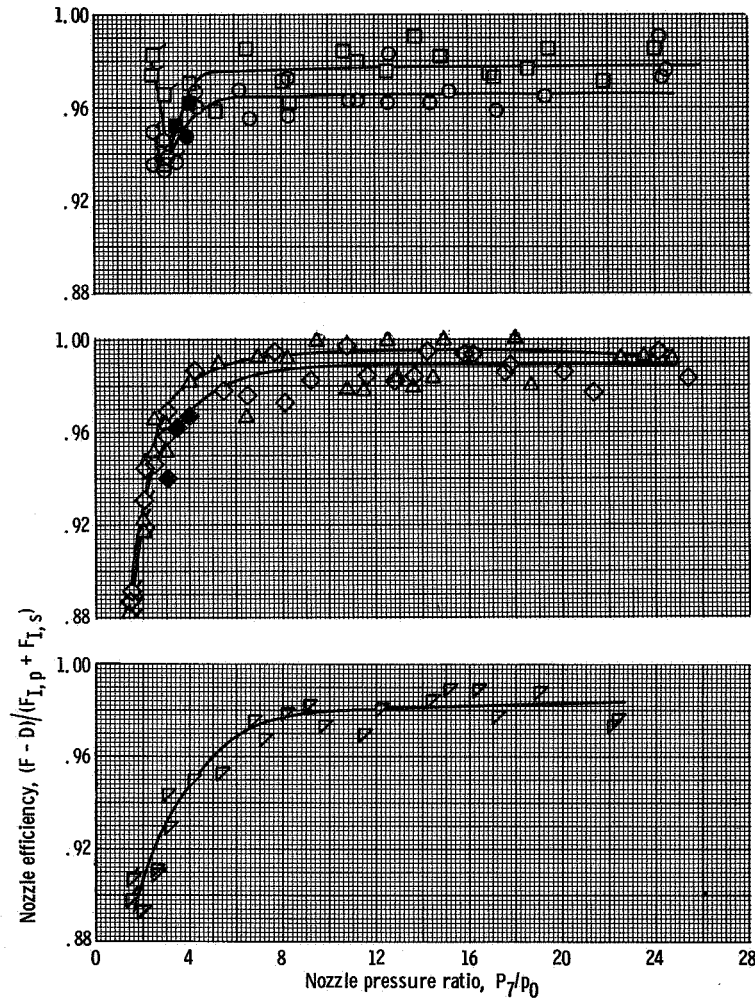


(b) Dry acceleration, configuration A.

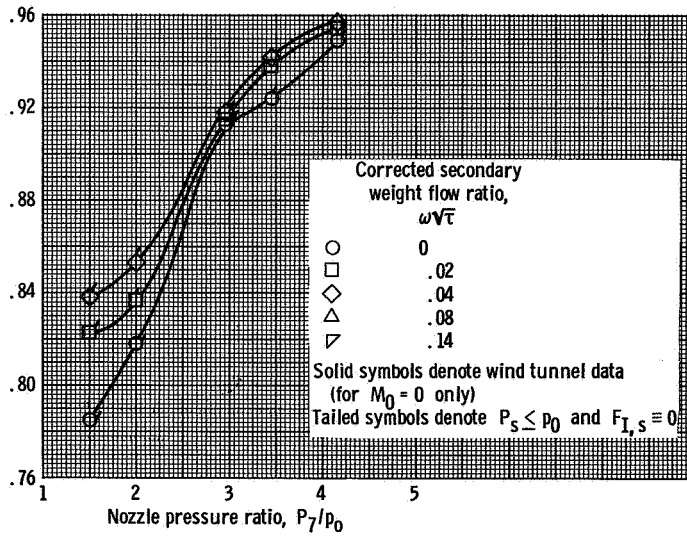


(c) Reheat acceleration, configuration B.

Figure 18. - Ratio of secondary total pressure to free-stream total pressure required for corrected secondary weight flow ratios at various free-stream Mach numbers.



(a) Free-stream Mach number, 0.



(b) Free-stream Mach number, 0.40.

Figure 19. - Nozzle efficiency as function of nozzle pressure ratio, configuration A.

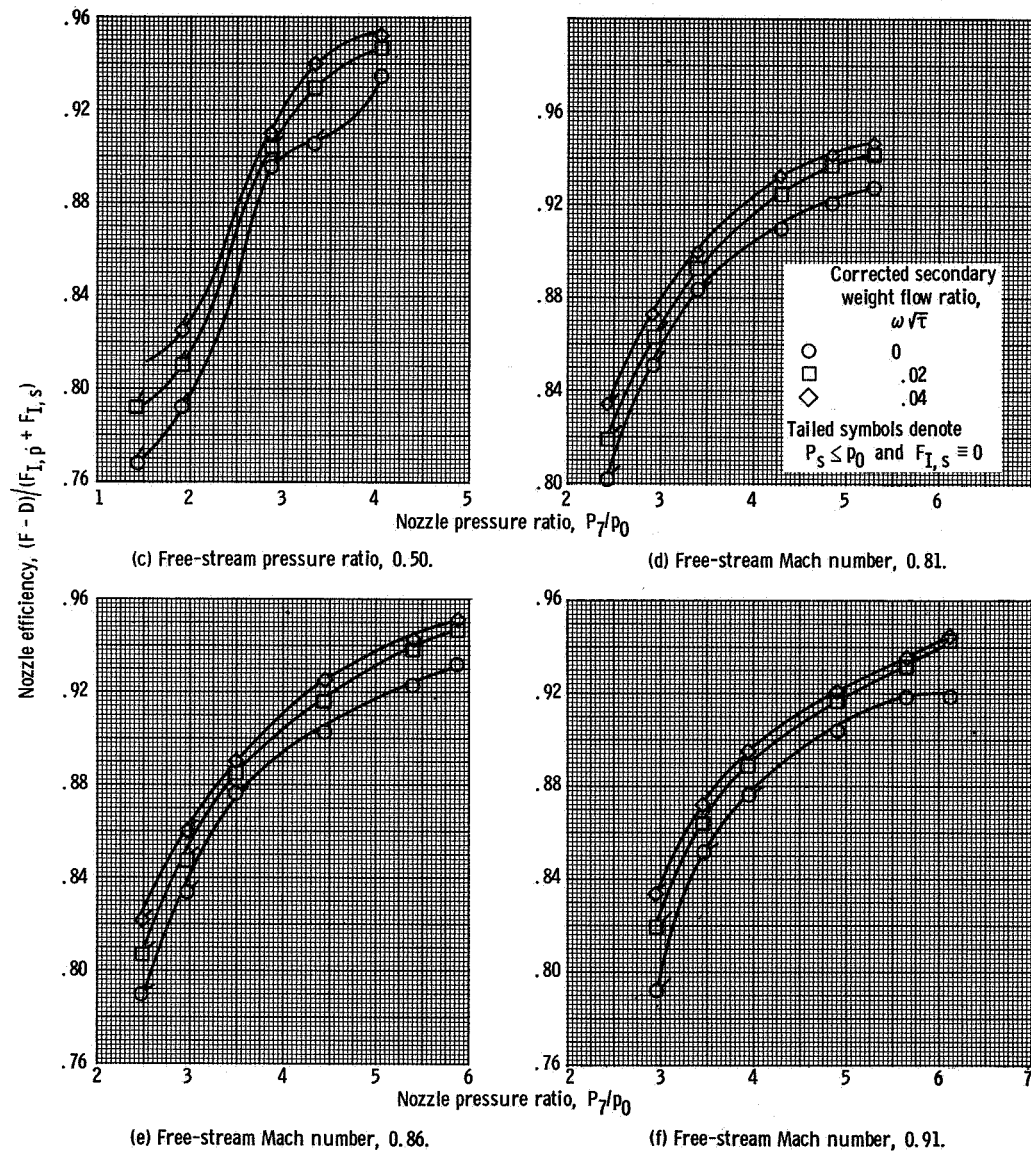


Figure 19. - Concluded.

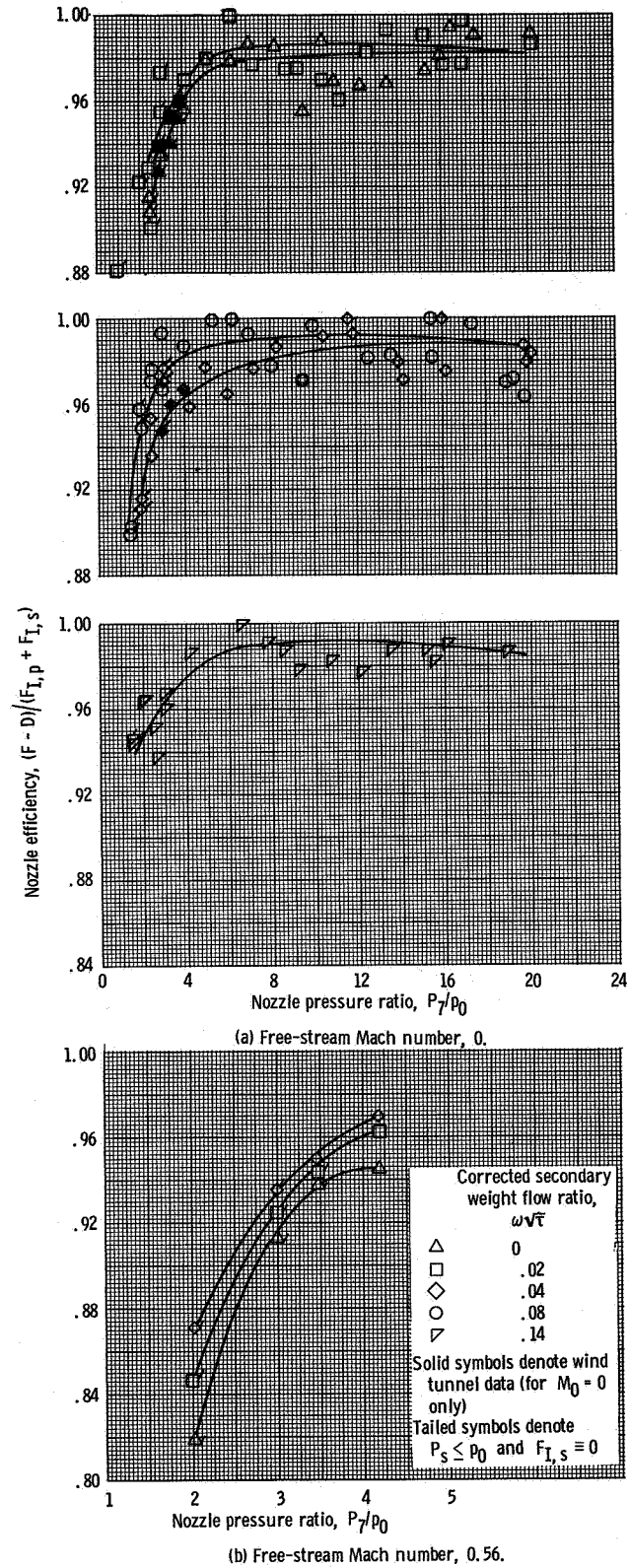
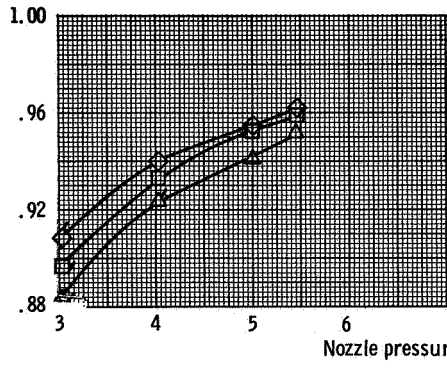
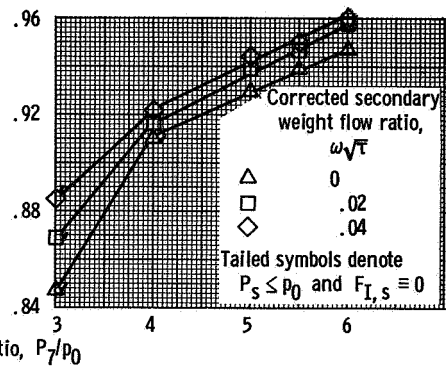


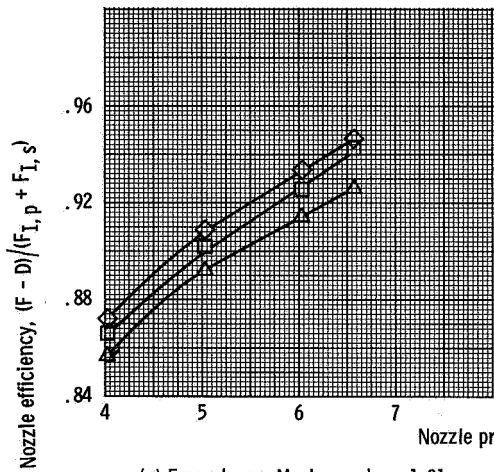
Figure 20. - Nozzle efficiency as a function of nozzle pressure ratio, configuration B.



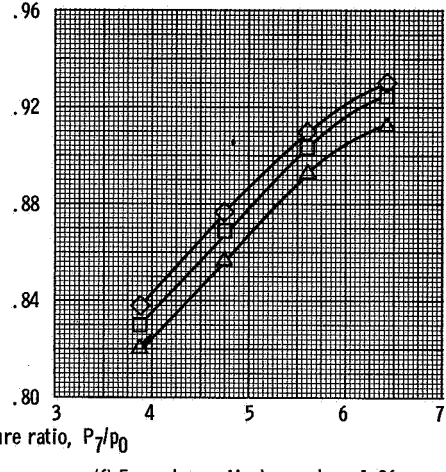
(c) Free-stream Mach number, 0.82.



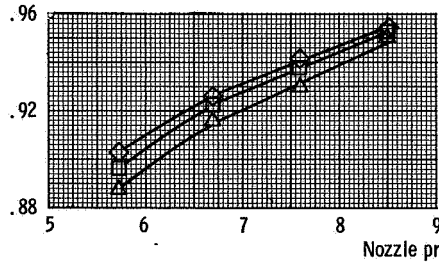
(d) Free-stream Mach number, 0.91.



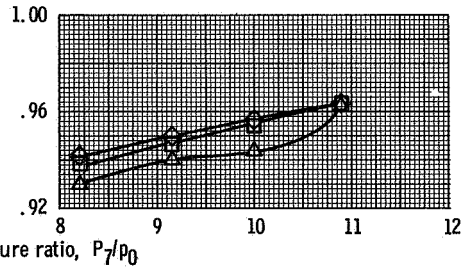
(e) Free-stream Mach number, 1.01.



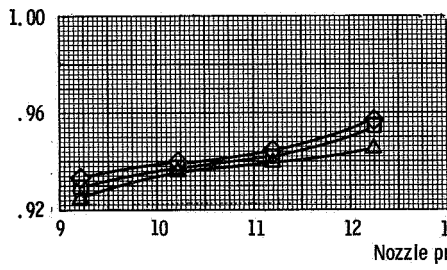
(f) Free-stream Mach number, 1.06.



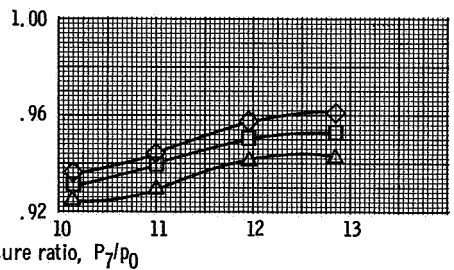
(g) Free-stream Mach number, 1.27.



(h) Free-stream Mach number, 1.57.

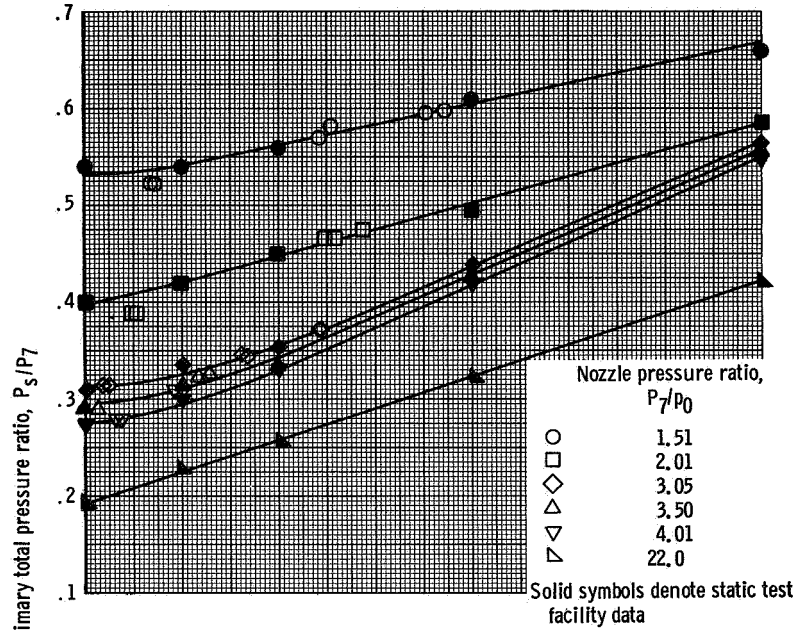


(i) Free-stream Mach number, 1.77.

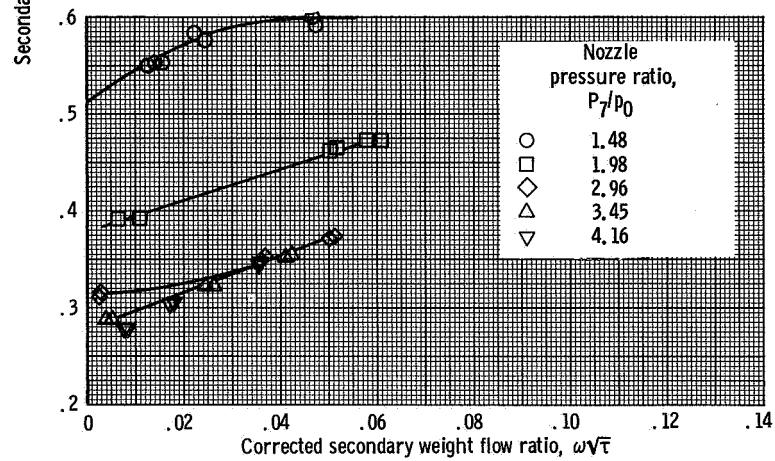


(j) Free-stream Mach number, 1.97.

Figure 20. - Concluded.



(a) Free-stream Mach number, 0.



(b) Free-stream Mach number, 0.40.

Figure 21. - Corrected secondary weight flow ratio as function of secondary to primary total pressure ratio for configuration A.

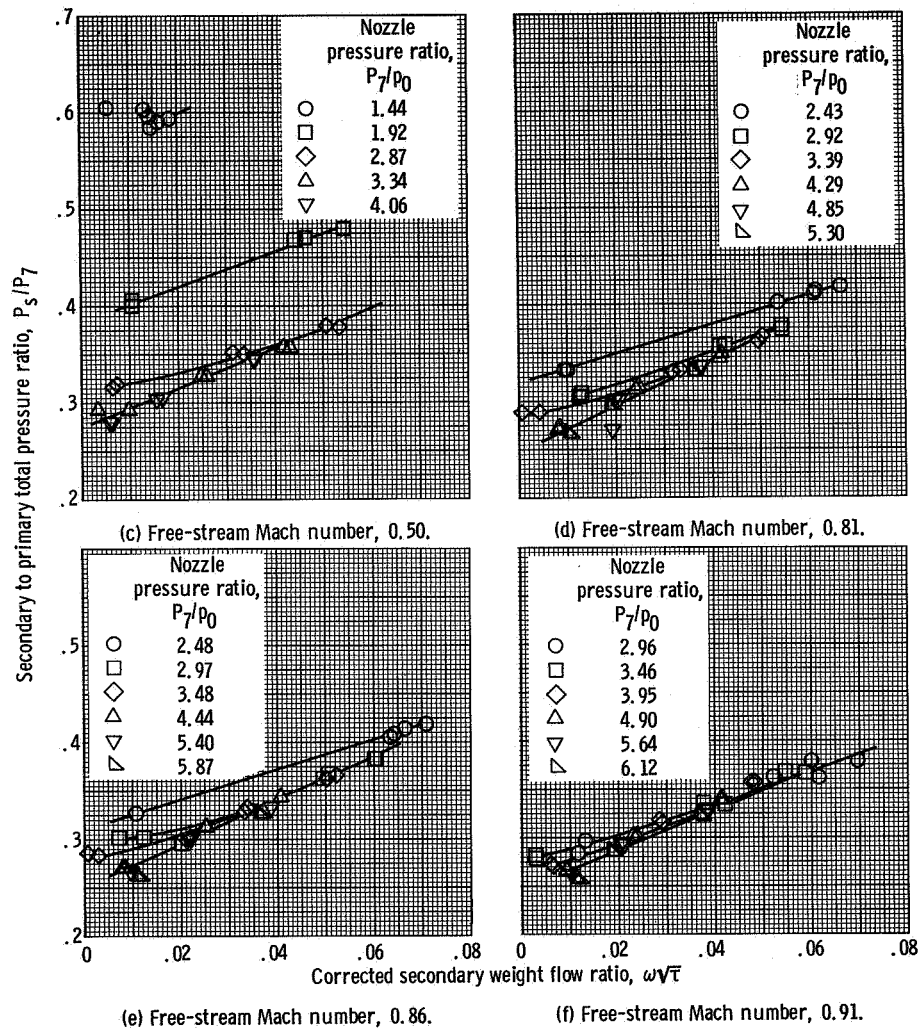


Figure 21. - Concluded.

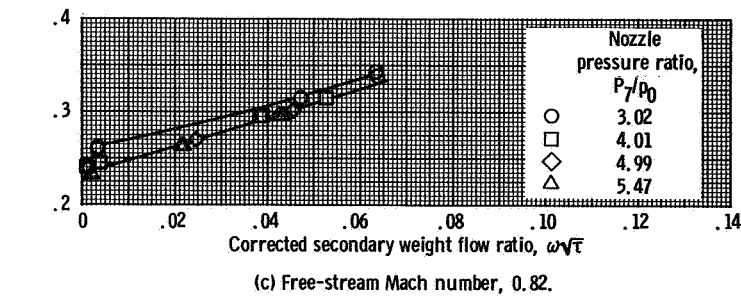
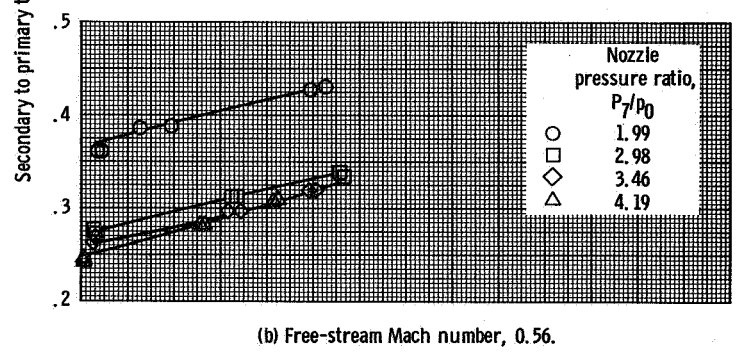
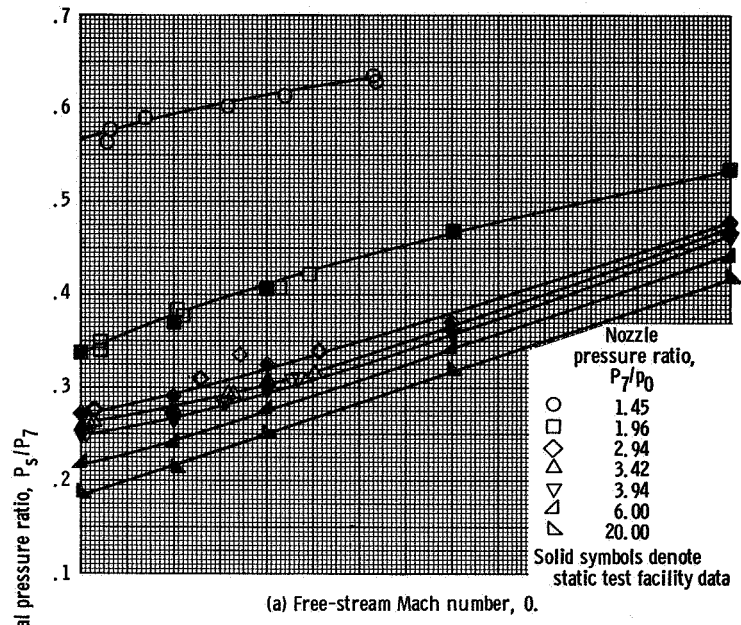
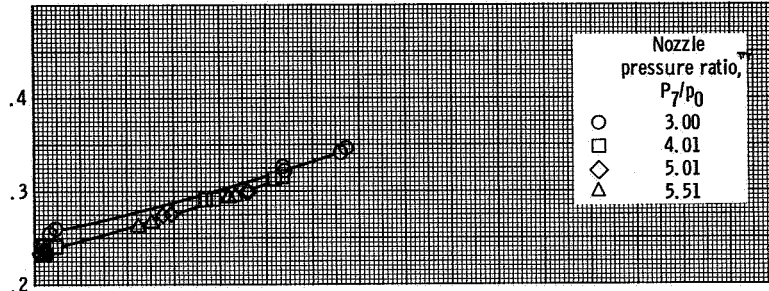
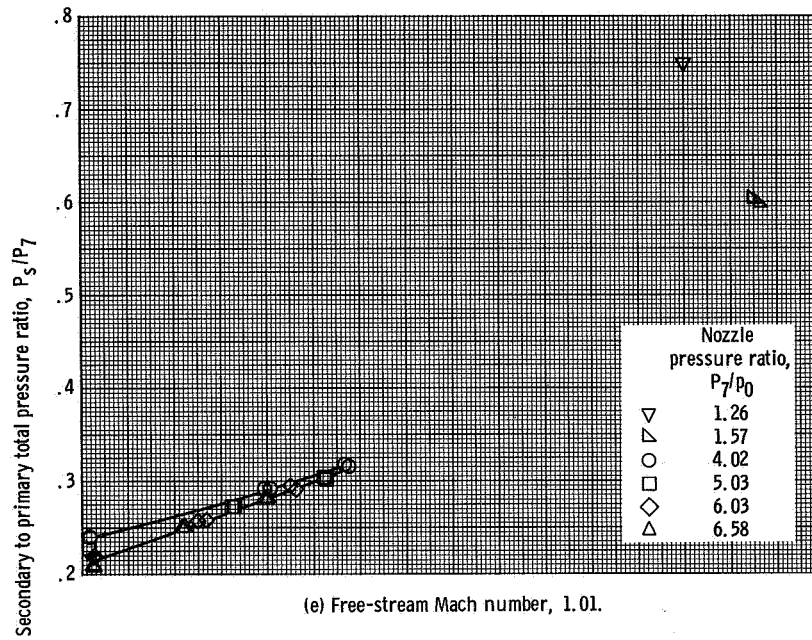


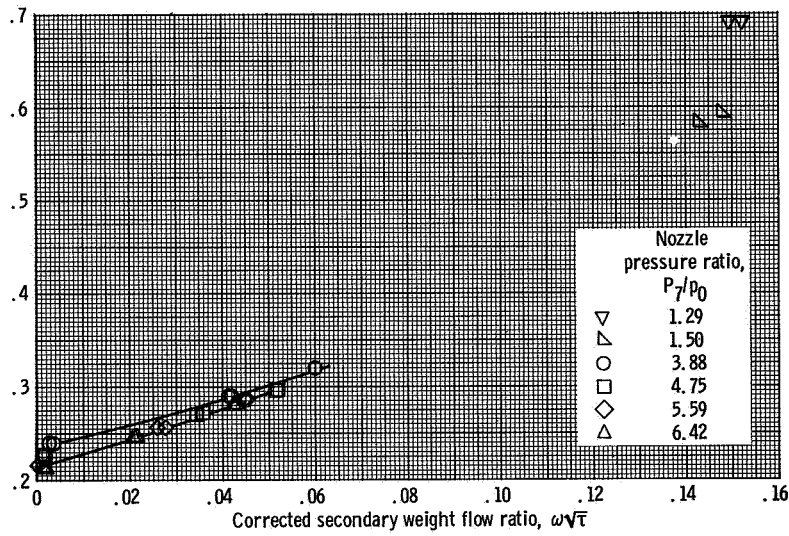
Figure 22. - Corrected secondary weight flow ratio as function of secondary to primary total pressure ratio for configuration B.



(d) Free-stream Mach number, 0.91.

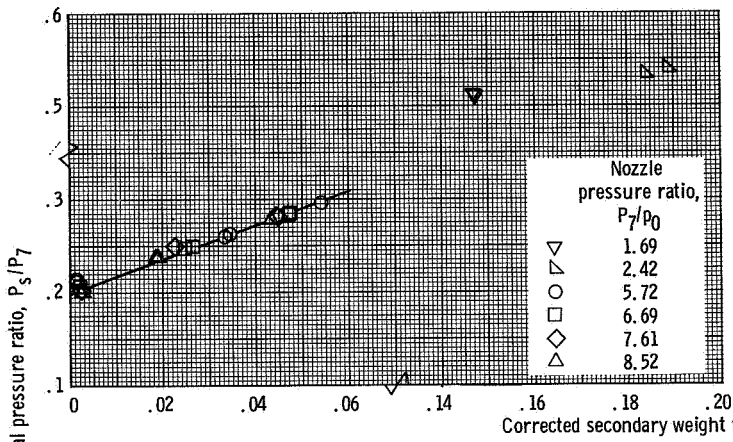


(e) Free-stream Mach number, 1.01.

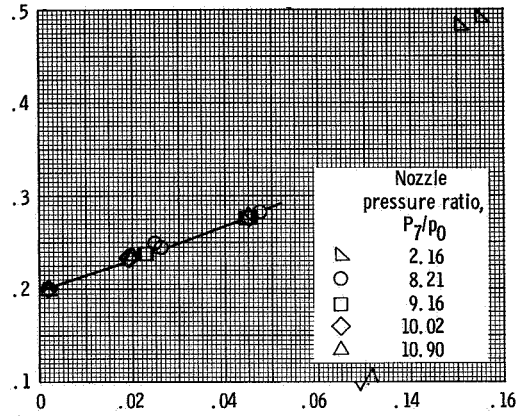


(f) Free-stream Mach number, 1.06.

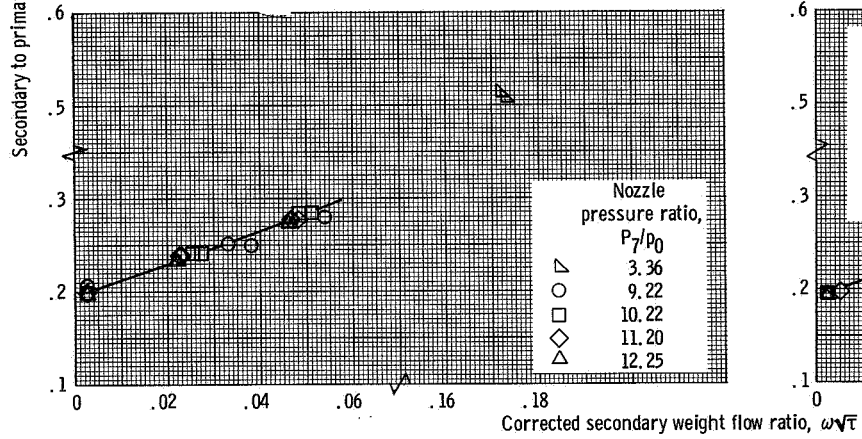
Figure 22. - Continued.



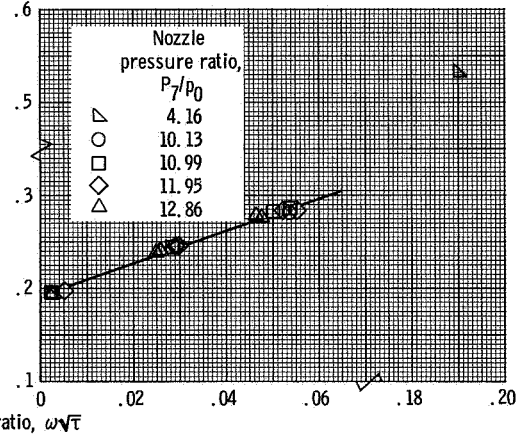
(g) Free-stream Mach number, 1.27.



(h) Free-stream Mach number, 1.57.



(i) Free-stream Mach number, 1.77.



(j) Free-stream Mach number, 1.97.

Figure 22. - Concluded.